Synchronous temperature variation monitoring during ultrasound imaging and/or treatment pulse application: a phantom study

Hermes A. S. Kamimura, *Member, IEEE,* Niloufar Saharkhiz, *Student Member, IEEE*, Stephen A. Lee, *Student Member, IEEE,* and Elisa E. Konofagou, *Senior Member, IEEE*

***Abstract*—Ultrasound attenuation through soft tissues can produce an acoustic radiation force (ARF) and heating. The ARF-induced displacements and temperature evaluations can reveal tissue properties and provide insights into focused ultrasound (FUS) bio-effects. In this study, we describe an interleaving pulse sequence tested in a tissue-mimicking phantom that alternates FUS and plane-wave imaging pulses at a 1 kHz frame rate. The FUS is amplitude modulated, enabling the simultaneous evaluation of tissue-mimicking phantom displacement using harmonic motion imaging (HMI) and temperature rise using thermal strain imaging (TSI). The parameters were varied with a spatial peak temporal average acoustic intensity (I_{spta}) ranging from 1.5 to 311 W.cm^{-2}, mechanical index (*MI*) from 0.43 to 4.0, and total energy (E) from 0.24 to 83 J.cm^{-2}. The HMI and TSI processing could estimate displacement and temperature independently for temperatures below 1.80°C and displacements up to ~117 µm (I_{spta}<311 W.cm^{-2}, *MI*<4.0, and E<83 J.cm^{-2}) indicated by a steady-state tissue-mimicking phantom displacement throughout the sonication and a comparable temperature estimation with simulations in the absence of tissue-mimicking phantom motion. The TSI estimations presented a mean error of ±0.03°C versus thermocouple estimations with a mean error of ±0.24°C. The results presented herein indicate that HMI can operate at diagnostic-temperature levels (i.e., <1°C) even when exceeding diagnostic acoustic intensity levels (720 mW.cm^{-2} < I_{spta} < 207 W.cm^{-2}). In addition, the combined HMI and TSI can potentially be used for simultaneous evaluation of safety during tissue elasticity imaging as well as FUS mechanism involved in novel ultrasound applications such as ultrasound neuromodulation and tumor ablation.**

***Index Terms*— Acoustic radiation force, harmonic motion imaging, thermal strain imaging, ultrasound neuromodulation.**

I. Introduction

The attenuation of ultrasonic waves in viscoelastic tissues leads to the generation of an acoustic radiation force (ARF) and tissue heating [1], [2]. Monitoring ultrasound-induced temperature and displacement of the tissue through ultrasound imaging enables the estimation of its properties and the evaluation of bio-effects of ultrasound [3]–[5]. The contribution of those effects influence the quantitative evaluation of the tissue mechanical properties in several ultrasound imaging modalities [6]–[12] and it can provide additional tools to help elucidating bio-effects such as focused ultrasound (FUS) neuromodulation [13]. Diagnostic to mild hyperthermia ultrasound pulses have been linked to hypotheses for the neuromodulation effects based on capacitance changes in the neuronal membrane produced by ARF-induced neuronal membrane deformation and/or thermal effects [13]. Magnetic resonance (MR)-based techniques such as MR-ARF imaging [14]–[16] and proton resonance frequency-shift thermometry [17]–[20] can be used to evaluate ARF and tissue heating simultaneously, but with increased costs and limited time resolution (4.7 s) [21].

During sonication, the tissue under stress moves in the direction of the FUS beam, causing a displacement proportional to the ARF amplitude. The ARF generated through the tissue absorption of the ultrasound wave can be defined by [1], [3].

$$F = \frac{2\alpha I}{c} \tag{1}$$

where I denotes the acoustic intensity field, α is the acoustic absorption coefficient, and c is the speed of sound. When the ARF ceases, an elastic restoring force due to tissue properties (Young's modulus) moves the tissue back in the opposite direction. The ARF-induced tissue motion is given by [22] as follows.

$$\rho \frac{\partial^2 \vec{u}}{\partial t^2} = \left(B + \frac{\mu}{3}\right) \vec{\nabla}\left(\vec{\nabla}.\vec{u}\right) + \mu \nabla^2 \vec{u} + \rho \overrightarrow{\boldsymbol{f_v}} \tag{2}$$

where ρ is the density of the medium, B is the bulk modulus, μ is the shear modulus, $\vec{u}$ is the induced displacement, and $\overrightarrow{\boldsymbol{f_v}}$ is the force vector per unit mass. The tissue motion can be modulated through the use of an amplitude-modulated (AM) ARF, such as in harmonic motion imaging (HMI) [23]. In HMI, the AM micron-scale tissue motion is estimated through RF phase-sensitive cross-correlation methods [24], [25]. The tissue responses to the ARF dynamic component include displacement, axial compressive strain, and changes in the relative phase shift that reveal viscoelastic tissue properties

This study was supported in part by National Institutes of Health (NIH) under award numbers R01CA228275 and R01EB027576, (Google) X, and Focused Ultrasound Foundation. The authors are with the Department of Biomedical Engineering, Columbia University, New York, NY 10027 USA (e-mail: ek2191@columbia.edu).

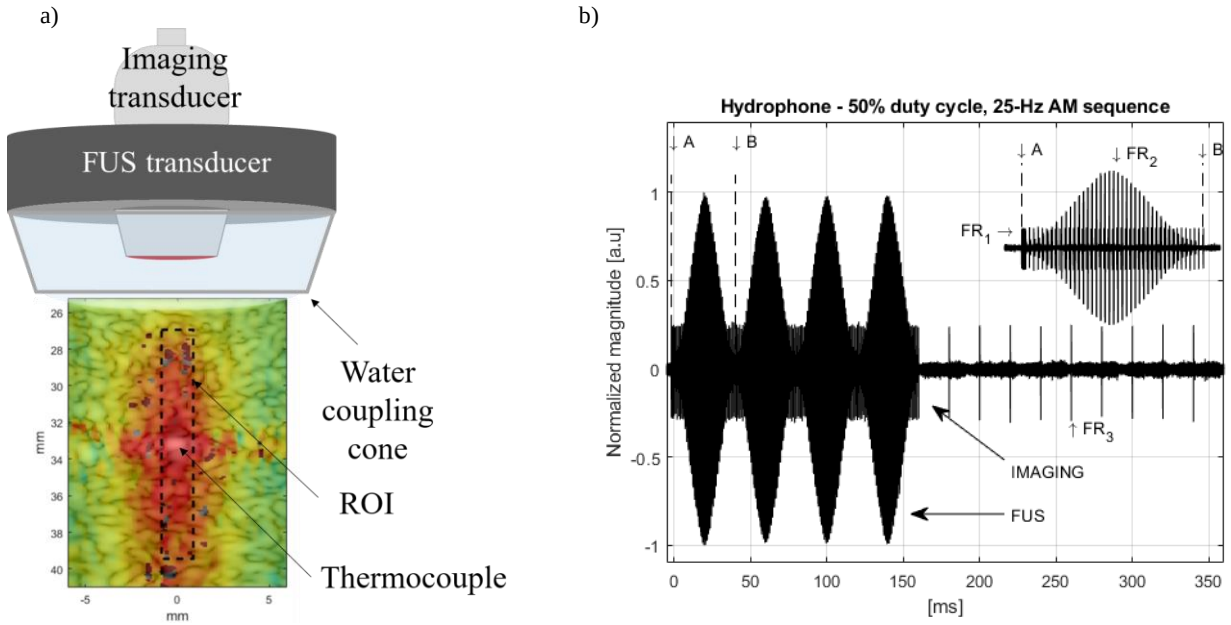

Fig. 1. Experimental setup and ultrasound pulse sequence. (a) The experimental setup comprises a 4-annular array FUS transducer coaligned with an imaging probe (P12-5) both driven by a Verasonics Vantage system. A water cone was used to acoustically couple the transducers with the phantom. A thermocouple was used to measure the temperature at the FUS focus. The picture shows an example of a displacement image generated by the acoustic radiation force. All analysis were performed within the ROI defined based on the FWHM hydrophone measurements in water. (b) Interleaved ultrasound pulse sequence observed in hydrophone acquisitions. The example shows four 25-Hz AM cycles generated by the FUS transducer and a magnification within the first AM cycle on the top right (A and B indicate the start and end times of the first AM cycle). Plane wave imaging sequences were acquired with sampling frequency of 14 kHz before the FUS pulses (FR_1), then at 1 kHz interleaved with the FUS pulses (FR_2), and finally at 100 Hz after the FUS pulses (FR_3). Please note that the image in Fig. 1(a) is not to scale and is exaggerated in size to provide the information needed.

[26], [27]. The estimation of these parameters holds promising clinical applications such as the detection of pathological tissues in humans, for example, tumors [28]–[31].

Conversely, the attenuation of the ultrasound wave in biological tissues can generate tissue heating. The volume rate of heat deposition assuming a peak pressure p_0 can be estimated by [2], [32]

$$Q = \alpha \frac{p_0^2}{\rho c} \tag{3}$$

In perfused tissues *in vivo*, the tissue heating can be estimated by the Pennes' bioheat transfer equation [33]

$$\rho C_t \frac{\partial T(\boldsymbol{r},t)}{\partial t} = k_t \nabla^2 T(\boldsymbol{r},t) + V \rho_b C_b \big(T_b - T(\boldsymbol{r},t)\big) + Q(\boldsymbol{r},t) \tag{4}$$

where C_t is the specific heat of tissue, T is the tissue temperature at a spatial coordinate $\boldsymbol{r}$ and time t, k_t is the tissue thermal conductivity, V is the perfusion rate per unit volume of tissue, ρ_b is the blood density, C_b is the blood specific heat, and T_b is the blood temperature. For non-perfused tissues, the maximum temperature at the focus can be estimated by $T_{max} = 2\alpha I/C_t$, with a temperature decrease following an exponential decay $\Delta T(t) = T_{max} e^{-(t-t_{end})/\tau}$, once sonication ends ($t_{end}$ is the time when sonication ends and τ is the time constant) [34]. As a result, high-temperature increases (>50°C) can cause tissue expansion and changes in tissue properties that can affect ultrasound-induced displacement [35].

Thermal strain imaging (TSI) is an ultrasound-based technique that evaluates the apparent displacement caused by temperature-induced sound speed changes in tissues [36]–[39]. TSI can potentially provide a quantitative assessment of tissue inflammation, metabolic rate, and thermal effects for treatment guidance during high-intensity FUS (HIFU) applications [40]. Intriguingly, the heating induced by the HIFU can generate not only apparent displacement but also tissue motion. Therefore, an evaluation of both tissue displacement and heating can provide important feedback for the evaluation of the tissue mechanical properties as well as a comparison of multiple factors present during the HMI and TSI acquisitions.

In this study, we investigated the displacement and temperature increase induced by FUS in a tissue-mimicking phantom using HMI and TSI. An interleaved pulse sequence was developed to alternate FUS pulses with plane-wave imaging and enable the operation of both FUS and imaging transducers by one dual-channel ultrasound research system. Thermocouple measurements were used to validate TSI measurements and compared with simulation results. The contribution of both temperature and displacement was evaluated across different acoustic intensities and ultrasound energies.

II. Materials and Methods

A. Experimental setup

A 4-element annular array transducer (center frequency: 1.10 MHz, frequency bandwidth: 0.88-1.32 MHz; HIFUPlex, Sonic Concepts Inc. Bothell, WA, USA) and a confocally aligned imaging transducer (104 elements, center frequency: 7.8 MHz, frequency bandwidth: 5-12 MHz; P12-5, ATL Philips, Bothell, WA, USA) were driven by an ultrasound research system (256-channel, HIFU configuration; Vantage, Verasonics, Kirkland, WA, USA). A coupling cone filled with deionized, degassed water coupled the transducers to a custom elasticity phantom (Young's modulus: 5 ± 1 kPa, speed of sound: 1530-1550 m/s, attenuation: 0.50 ± 0.05 dB/cm at 1 MHz; custom model, CIRS, Norfolk, VA, USA) (Fig. 1a). A needle thermocouple (T-type, 0.25 mm diameter; Omega Engineering Inc., Norwalk, CT, USA) inserted in the phantom recorded in real-time the temperature at the FUS focus using a data logger at a 2 kHz sampling rate (model DI-245, DataQ Instruments, Akron, OH, USA). The tip-sensitive part of the thermocouple was targeted using B-mode and displacement imaging [41], [42] (Fig. 1a). At the end of the sonication, the peak temperature was estimated following the suppression of the viscous-heating artifact originated by the thermocouple and phantom tissue interaction using an iterative curve fitting method based on the Bioheat equation (Eq. 4). Further details can be found in [43]. Briefly, successive curve fittings were performed with the starting point moving at each iteration until the maximum R^2 indicated a negligible viscous heating artifact. The temperature was then back estimated at the initial starting point. All devices were controlled with customized Matlab scripts (Matlab 2018b, MathWorks, Natick, MA, USA).

B. Ultrasound pulse sequence

The pulse sequence consisted of AM excitation pulses generated by the FUS transducer interleaved with monitoring plane-wave imaging pulses generated by the imaging transducer (Fig. 1b). The AM transmit signals were generated by the Vantage system. Each AM cycle was generated by forty evenly-spaced rectangular voltage pulses with a relative pulse width proportional to ½ $\sin^{-1} f_{AM}$, where f_{AM} is the AM frequency, equal to 25 Hz. The duty cycles used in the excitation pulses were 10%, 50%, and 75%, using a fixed pulse repetition frequency (PRF) of 1 kHz. The number of AM cycles were 4 or 10 with derated pressure levels of 2.0, 3.1, and 4.2 MPa at a FUS frequency f = 1.10 MHz (fundamental frequency of the FUS transducer) and 0.80, 1.3, and 1.7 MPa at f = 3.57 MHz (3rd harmonic of the FUS transducer). Therefore, the parameter space for the excitation pulses covered a spatial-peak temporal average acoustic intensity (I_{spta}) ranging from 1.5 to 311 W.cm^{-2}, mechanical index (MI) from 0.43 to 4.0, and total energy from 0.24 to 83 J.cm^{-2} (supplementary material - Table I). The power-law frequency-dependent acoustic attenuation was assumed equal to $\alpha = 0.057 f^{0.90}$ (in Np/cm). The total energy E was defined as the I_{spta} multiplied by the AM excitation duration, 160 or 400 ms, for 4 and 10 AM cycles.

The RF data acquisitions using ultrasound plane-wave imaging were performed at variable frame rates (Fig. 1b). First, a baseline acquisition before the AM excitation pulses was performed at a frame rate of FR_1 = 14 kHz during 1 ms

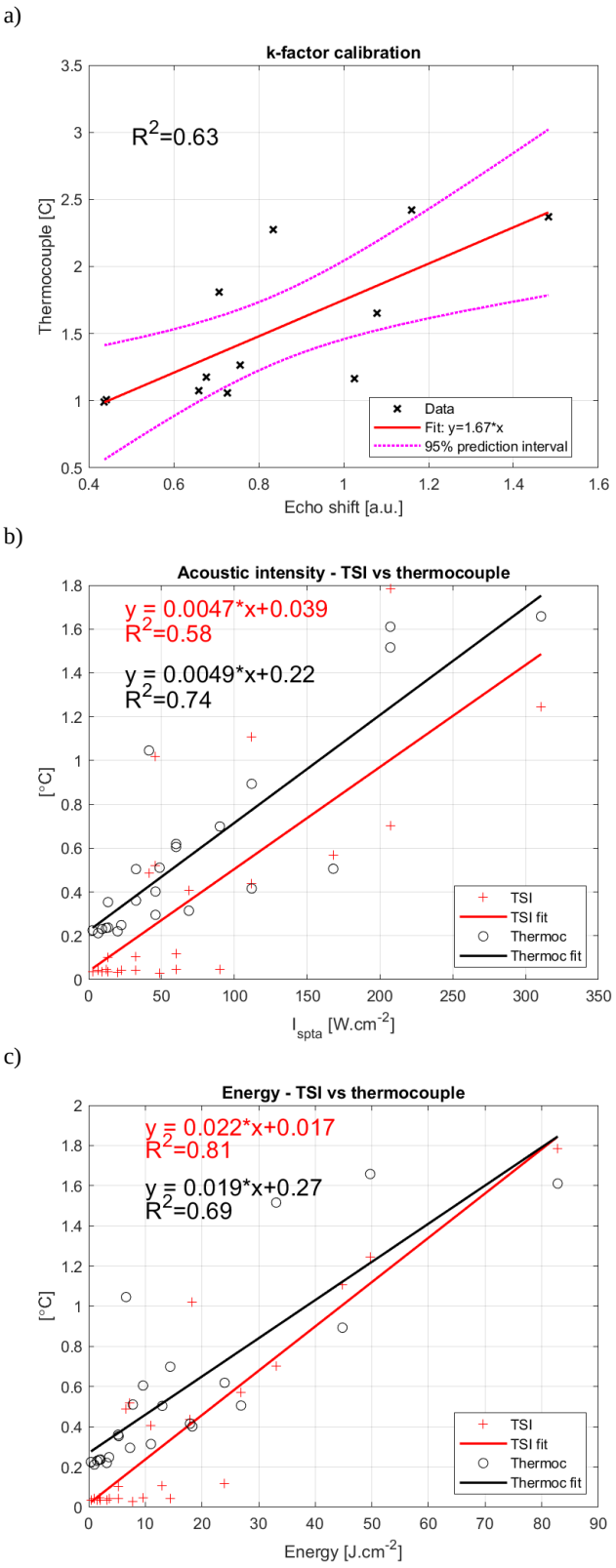

Fig. 2. Thermocouple measurements and TSI calibration. (a) *k*-factor determined by the linear regression of thermocouple and TSI acquisitions using k = 1. TSI temperature evaluation compared with thermocouple estimation when varying (b) the spatial-peak-temporal average acoustic intensity (I_{spta}) and (c) the total energy (E) of the pulse.

a)

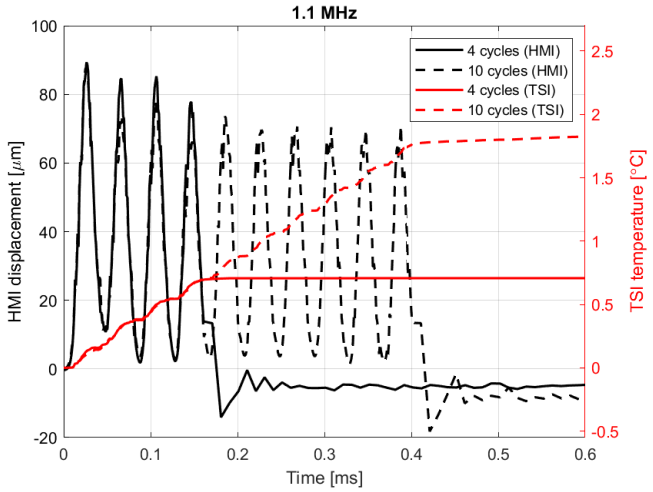

b)

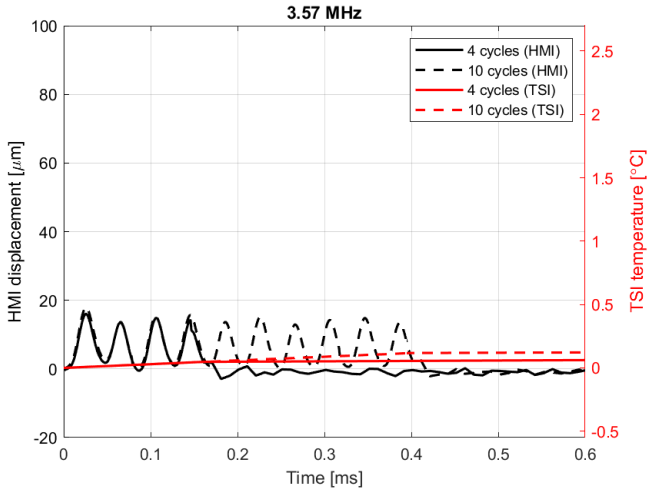

Fig. 3. Frequency-dependent considerations in simultaneous displacement and temperature estimation. The sequences consisted of interleaved HMI displacement and TSI temperature estimations for (a) 1.10 MHz using I_{spta} = 207 W.cm^{-2} and E = 33 J.cm^{-2} (4 cycles) and 83 J.cm^{-2} (10 cycles) and (b) 3.57 MHz, using I_{spta} = 34 W.cm^{-2} and E = 5.4 J.cm^{-2} (4 cycles) and 14 J.cm^{-2} (10 cycles). The 4 or 10 AM cycles at 25 Hz resulted in pulse durations of 160 ms or 400 ms, respectively.

(equivalent to 14 frames). Then, image acquisitions were interleaved with the AM excitation pulses at a frame rate of FR_2 = 1 kHz during the AM excitation pulses (160 ms for 4 AM-cycles and 400 ms for 10 AM-cycles). Finally, a lower frame rate of FR_3 = 100 Hz was used for post-AM pulse monitoring.

C. Harmonic Motion Imaging

The mean HMI displacement was estimated by first applying delay-and-sum beamforming to the RF data. Then, the AM excitation pulse interference was suppressed using a 2nd order Butterworth notch filter applied over the n harmonics of the excitation pulse, where $n*f \pm \Delta f$; with n = 1 to 5 for f = 1.10 MHz, and n = 1 to 3 for f = 3.57 MHz; and Δf bandwidth of 500 kHz around the harmonic frequency. Finally, the axial displacement was estimated using a normalized 1-D cross-correlation estimation between the average of the baseline frames (14 frames before the AM excitation pulses) and subsequent frames acquired during and after the excitation pulses. Values with correlation coefficients below 0.90 were disregarded. Then, a 3-by-3 median filtering operation was applied. All analyses were performed offline within a region of interest (ROI) defined by the -3 dB focus region estimated by hydrophone measurements in water (model HGL-0200, ONDA Corp., Sunnyvale, CA, USA). At 1.10 MHz, the ROI was 1.2 by 12.5 mm and, at 3.57 MHz, 0.4 by 4.8 mm.

D. Thermal Strain Imaging

The TSI processing shares the same initial steps with HMI, up to where the inter-frame displacements were obtained. Following that, the cumulative displacement was calculated by summing up the inter-frame displacements. Then, a 3-by-3 median filter, a 2-D Gaussian filter using a 3-by-1 axis-aligned anisotropic smoothing kernel, and an averaging filter were applied to the data to suppress high-frequency components of the displacements [40], [44]. The temperature mapping was estimated recursively by first determining the echo shifts induced by the FUS along the axial direction relative to the average baseline frame, assuming a k-factor equal to 1.

$$\Delta T(z,y,t) = k\frac{\partial(\Delta d)}{\partial z} \quad (5)$$

The k-factor was then determined based on the linear regression of the temperatures measured by a thermocouple $\Delta T(z,y,t)$ and the echo shift $\frac{\partial(\Delta d)}{\partial z}$ estimated by TSI with k = 1 [45]. The final TSI images were obtained by re-running the processing with the calibrated k-factor found in this step.

E. Temperature simulation

To determine the expected temperature in the absence of tissue motion, the heating and heat diffusion in the phantom were simulated without an acoustic radiation force on the Matlab k-wave Toolbox [46] using the Pennes' bioheat equation [33], [47], assuming a homogeneous medium. The perfusion term in Eq. 4 was zeroed, so only heat diffusion was considered. The normalized FUS acoustic pressure maps obtained from hydrophone measurements in water were used to define the steady-state pressure distribution at 1.10 MHz and 3.57 MHz. The amplitude of the normalized pressure maps was then modulated at 25 Hz and discretized in 41 maps with a pulse repetition frequency of FR_2 = 1 kHz, and other parameters including duty cycle, pressure amplitude, and pulse duration following the same sequences adopted in the experiments (section II.B and supplementary material - Table 1). The volume rate of heat deposition in the phantom was defined as $Q = \alpha p_0^2/(\rho c)$ (Eq. 3), using the following properties [48], c = 1530 m/s, ρ = 1000 kg.m^{-3}, α = 0.55 dB.cm^{-1} at 1 MHz, C_t = 3.5 kJ.kg^{-1}C^{-1}, k_t = 0.50 W.m^{-1}C^{-1}, and a power-law absorption exponent equal to 0.90. The initial temperature was set to 22°C, and a 5 kHz sampling rate was used to record the temperature during sonication.

III. Results and Discussion

This study evaluated the temperature increase induced by ultrasound absorption in a tissue-mimicking phantom material

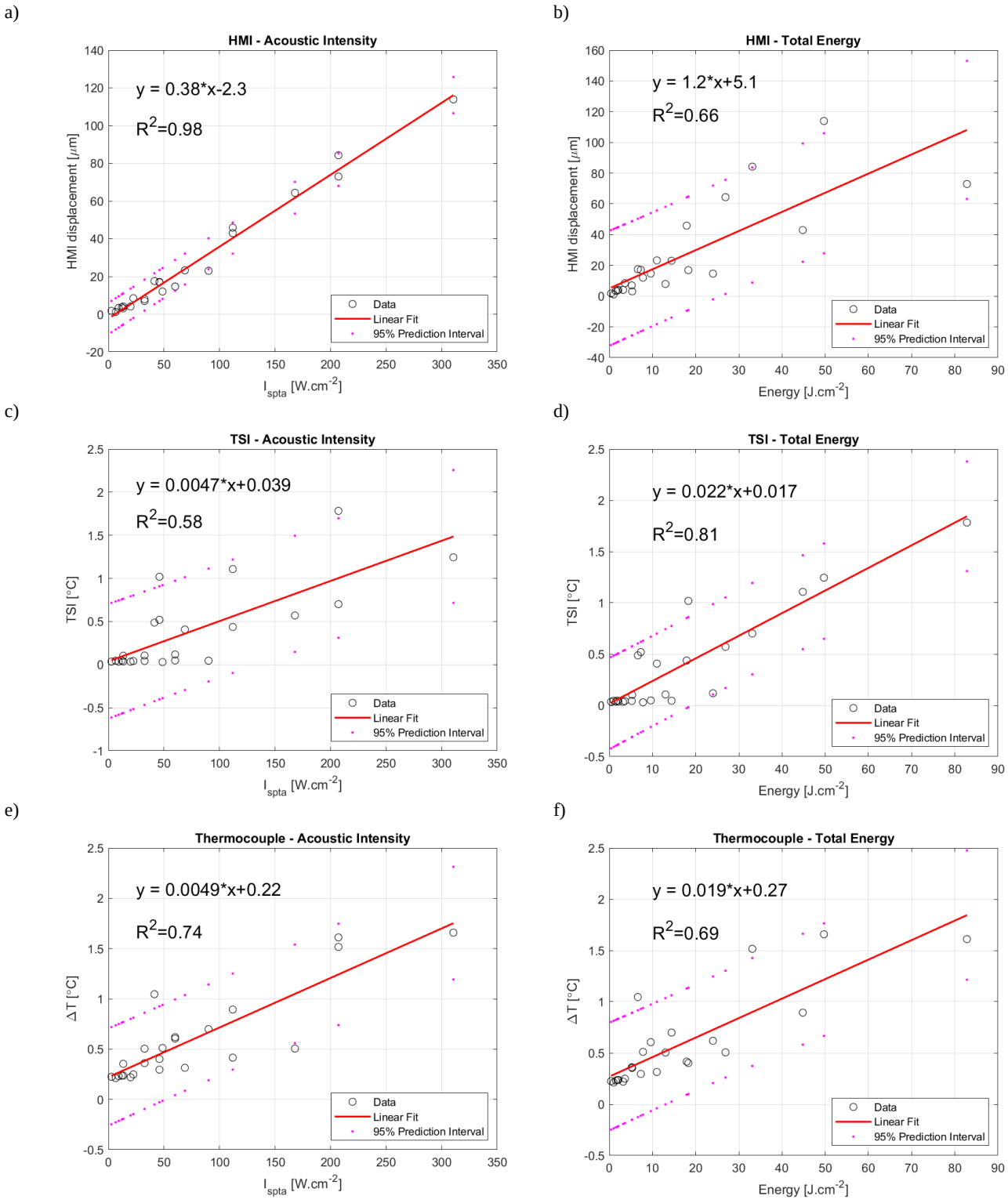

Fig. 4. The overall results obtained experimentally in phantom using different I_{spta} and E levels with (a, b) HMI, (c, d) TSI, and (e, f) thermocouple measurements. The linear fittings show that HMI displacements present a more robust trend with I_{spta} (mean standard deviation of the error $\sigma_{I\text{-}HMI}$ = ±4.2 µm) than that with E ($\sigma_{E\text{-}HMI}$ = ±18.8 µm). The TSI temperature presented a slight better robustness with E vs I_{spta} ($\sigma_{I\text{-}TSI}$ = ±0.3°C vs $\sigma_{E\text{-}TSI}$ = ±0.2°C). The thermocouple measurements presented similar trends with I_{spta} and E ($\sigma_{I\text{-}Th}$ = ±0.2°C vs $\sigma_{E\text{-}Th}$ = ±0.3°C).

during an HMI sequence. The ultrasound attenuation generates both an ARF and tissue heating. A plane-wave imaging sequence was interleaved with FUS pulses, allowing both temperature evaluation through TSI and displacement through HMI.

The first step of the processing was the calibration of the TSI using thermocouple measurements. Fig. 2a shows the linear

regression fit obtained from the echo shifts detected by TSI (using $k = 1$) and thermocouple temperature measurements. The slope obtained from the fitting provided the corrected *k*-factor (Eq. 5), which calibrated the TSI for temperature measurements in the °C unit. Multiple reasons can explain the higher variability in the k-factor calibration plot using the thermocouple (Fig. 2a) in comparison to previous studies in phantoms [39], [40], [45], [49]. First, longer sonications that enable achieving heating levels of several degrees Celsius (i.e., 300 s, 20°C) are less susceptible to viscous heating artifacts since their contribution decays over time [50], [51]. Despite efforts to reduce the artifacts using our previously demonstrated iterative curve fitting method [43], some degree of variation in the standard deviation is expected (up to 38% for the thermocouple and low-temperature levels in this study). Some studies employed a long pause between the end of the sonication and the TSI acquisitions (i.e., 1.1 s to 1.5 s [39]). This approach allows a more stable estimation of temperature but also may not account for the temperature decay by diffusion between the time of the end of sonication and the time at which the TSI assesses the temperature. The *k*-factor calibration can also be obtained using a heated water tank [45], which elevates the temperature of the phantom without an ultrasound heating source. Thus, the estimation of temperature is also more stable. Our study utilized the FUS as the heating source for the *k*-factor calibration because this approach seems to be more feasible for *in vivo* applications in our future studies. For example, we can gradually and locally heat human tissue to obtain the echo shifts. Finally, the interleaved sequence we demonstrated here allows the assessment of displacement, which cannot be assessed using the long-pause approaches.

Tissue motion may impose limitations to the calibration of the *k*-factor *in vivo* since decorrelation may occur when using reference frames acquired at the beginning of sonication prior to a tissue motion event. This limitation can be critical, especially in long sonication protocols, such as in ablation. However, for short pulses (millisecond range at 1 kHz PRF), as we demonstrate in this study, the calibration should not be affected to the same extent as by tissue motion since the time scale of the respiratory motion, and other sources of motion *in vivo* are in the sub-Hz to Hz-range. Thus, our method has great potential to provide reasonable estimations of transient temperatures generated by short FUS pulses employed in applications such as ultrasound imaging and neuromodulation. Future studies will determine specific parameters that are more suitable for *in vivo* applications.

The calibrated TSI measurements were compared with the thermocouple measurements, where both acoustic intensity (Fig. 2b) and total energy (Fig. 2c) showed a linear relation. For both temperature plots using I_{spta} (Fig. 2b) and E (Fig. 2c), it can be seen that the TSI failed to measure temperatures below 0.4°C. This is a limitation of our interleaved method. After reaching the 0.4°C threshold, the measurements become less noisy, especially when using energy as an index for the temperature estimation (Fig. 2c). This is expected since I_{spta} takes into account the duty cycle but does not consider the duration of the sonication, whereas the energy E is directly proportional to the sonication duration (i.e., 160 ms for 4 AM-cycles or 400 ms for 10 AM-cycles). The results demonstrate that the TSI enabled temperature evaluations from 0.40 to 1.8°C. Our calibration method and interleaved imaging sequence add uncertainties to the measurements but also present several opportunities, such as the assessment of displacement and temperature during the AM pulse. This has important implications, such as in mechanistic studies for ultrasound neuromodulation that we will explore in future studies.

Fig. 3 shows examples of simultaneous evaluation of the average displacement and temperature within the ROI during sonications at 1.10 MHz using I_{spta} = 207 W.cm^{-2} and E = 33 J.cm^{-2} (4 cycles, 160 ms) and 83 J.cm^{-2} (10 cycles, 400 ms) and at 3.57 MHz using I_{spta} = 34 W.cm^{-2} and E = 5.4 J.cm^{-2} (4 cycles, 160 ms) and 14 J.cm^{-2} (10 cycles, 400 ms). The HMI displacement for both sonication durations was accompanied by a cumulative temperature increase but no significant increase in the displacement amplitude over time. A transient displacement in the first AM pulses was observed for higher acoustic intensities (i.e., first 4 HMI displacement cycles in Fig. 3a) followed by a steady-state (i.e., from the 5th to 10th cycles in Fig. 3a). Lower acoustic intensities showed a steady-state phantom tissue oscillation throughout the pulse sequence (Fig. 3b). In these representative cases, we can observe a reasonable relationship between I_{spta} (34/207 = 0.16) and average displacement of 14.6 ± 1.4 µm and 70.6 ± 1.5 µm generated by the low and high-intensity cases, respectively. The difference can be explained by the high uncertainties observed by tightly focused beams [52]. These trends were consistent for all HMI displacements explored in the parameters space of this study. As described previously, changes in ultrasound attenuation [53] and viscoelasticity of tissues for temperatures below the ablation threshold (up to 45°C) do not significantly affect the HMI-induced tissue displacement (<0.1%) [35]. This is consistent with the steady-state displacement observed herein, showing that the cumulative temperature increase did not affect the displacement estimation. Based on Suomi *et al*. [35], a significant change in the displacement is expected when a lesion with increased stiffness is formed for temperatures ranging from 50°C to 70°C. The results presented herein provide complementary information for the HMI assessment at low temperatures (up to 1.8°C), indicating that HMI can operate at temperatures considered safe for diagnostic ultrasound (i.e., <1°C) even when exceeding acoustic intensities above the imaging limits (720 mW.cm^{-2}<I_{spta}<207 W.cm^{-2}). Similarly, interleaving TSI with ARF sequences can potentially provide a safety evaluation for other ARF-based techniques such as ARF impulse imaging [54].

Both displacement and temperature increased linearly with the acoustic intensity and energy (Fig. 4). Particularly for TSI, the total energy was a slightly better predictor for thermal effects as the sonication duration dictates the temperature increase (Fig. 4d), as opposed to the acoustic intensity that does not take into account the pulse duration (Fig. 4c). The estimated standard deviation of the error for intensity $\sigma_{I\text{-}TSI}$ was ± 0.3°C versus for energy $\sigma_{E\text{-}TSI}$ equal ± 0.2°C. Conversely, the HMI displacements presented a more robust trend with I_{spta} (Fig. 4a) with a mean, standard deviation of the error $\sigma_{I\text{-}HMI}$ = ± 4.2 µm than that with E (Fig. 4b), with a mean, standard deviation of the error $\sigma_{E\text{-}HMI}$ = ± 18.8 µm. Lower intensity levels did not show strong transients effects in the displacement (Fig. 3b). The steady-state for both higher and lower intensities suggests that

a)

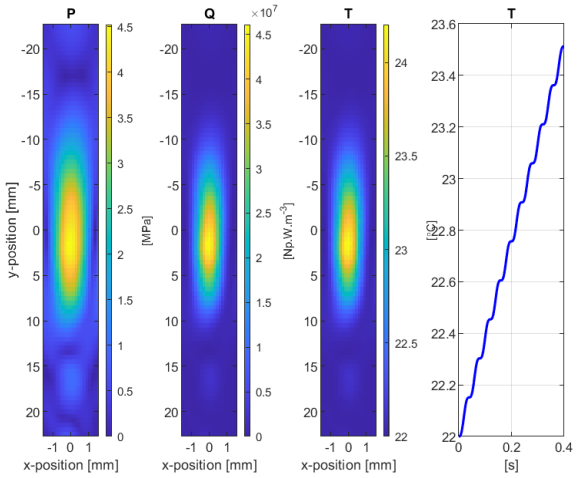

b)

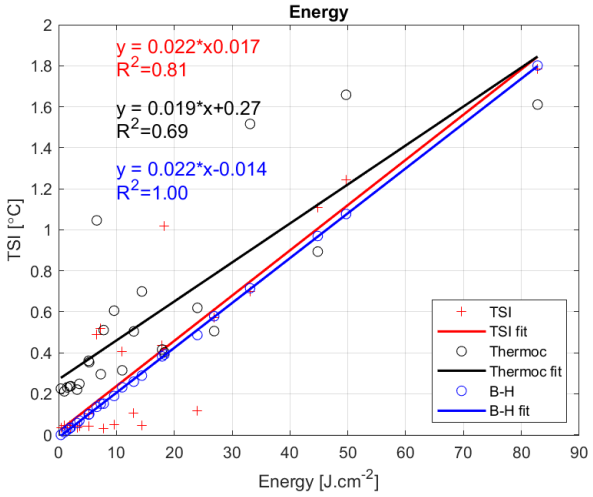

Fig. 5. (a) Temperature simulations, with examples of a pressure map *P* obtained with a hydrophone in free water, *Q* the volume rate of heat deposition, and *T* the temperature map, with the temporal series of *T* during a 400 ms pulse duration. (b) Comparison of thermocouple measurements and TSI estimations with the simulated temperature in phantom. The TSI estimation presented a lower mean error of ±0.03°C versus the thermocouple estimations ±0.24°C, when comparing with the simulated values.

the phantom attenuation and viscoelasticity were not significantly affected by the temperature ranges explored here.

Despite the low interference of temperature in the HMI displacement evaluation (including close-to-ablation levels by previous studies [35]), the effect of displacement in the TSI temperature estimation requires careful consideration. The TSI processing is based on estimating an apparent displacement due to changes in the tissue speed of sound caused by temperature increase. The calculation of the apparent displacement is based on a cross-correlation method and requires high correlation between consecutive RF signals for proper estimation. To evaluate the TSI performance, simulations were performed to estimate the temperature in the absence of tissue-mimicking phantom motion. Fig. 5a shows an example of the volume rate of heating deposition *Q* and the estimated temperature map *T* obtained from a pressure distribution *P* found in free water measurements with the hydrophone. The estimated temperature shown in plot *T* in Fig. 5a shows an example of a time series of the simulated 10-cycle temperature oscillation that resulted in a similar pattern observed in the experiments (Fig. 3). The interleaved TSI presented an average of 4.5±1.5% offset in the individual readings of temperature estimation compared to simulations of temperatures above the TSI threshold of 0.4°C (Fig. 5b). A comparison between experimental and simulation results shows that the TSI provides a more stable evaluation of the temperature than thermocouples. The results from the fittings show that the TSI estimation presented a lower mean error of ±0.03°C versus the thermocouple estimations ±0.24°C. The higher oscillations in the thermocouple estimations occur due to viscous heating artifacts that can be minimized [43], [55], but not completely removed in some cases. Thus, HMI displacements up to ~117 µm and TSI temperatures below 2°C can be estimated independently using the sequence demonstrated in this study. For higher pulse intensity, including ablative FUS pulse sequences [56]–[59], a careful evaluation is required, since much higher transient tissue motion is expected and a characterization of the change of tissue attenuation as a function of temperature is required for the correct evaluation of each effect [60]. For example, in HIFU pulse sequences, both simulation and TSI estimations can be corrected with a temperature-dependent β absorption coefficient [61], such as Q can be given by $Q=\beta f p^2/(\rho c)$ [32]. Sequence optimizations, for example, exploring the steady-state phase, can potentially minimize HMI effects on TSI. The combination of TSI and HMI can provide complementary evaluation of the tissue before ablation with TSI and during ablation with HMI. Such application will require a real-time implementation of the sequence presented herein. Future studies will explore the feedback of the biological tissue properties and the treatment's progress with the combined real-time TSI and HMI using FUS sequences with longer sonications and ablative temperatures.

Finally, ultrasound neuromodulation studies may also benefit from the pulse sequence and monitoring methods described here. Among the hypotheses for the neuromodulation effects of ultrasound, ARF has been associated with neuronal membrane activity changes. Tissue displacement imaging can be used as an index for ARF, and it has been shown extremely valuable for nerve targeting and mechanisms investigation [41], [42]. In addition, temperature changes can modify the membrane conductance, which can be generated by multiple sources such as light [62], electrical current [63], [64], and ultrasound [65]. Other hypotheses involving thermal effects, such as the soliton model, have also been discussed as potential ultrasound neuromodulation mechanisms [13], [66]. We have shown protocols that can provide high spatial specificity in both brain [67] and peripheral nerve stimulation [65], which involves temperature elevation [43] or, primarily, ARF in the brain [68] and nerves [69]. Therefore, the interleaved evaluation of displacement and temperature during the pulse, instead of a second or longer after the sonication is completed [49], [70], is essential to help elucidate the contribution of heating and ARF in ultrasound neuromodulation. The parameter space demonstrated here falls within a broad range of ultrasound neuromodulation studies [13]. Future studies will also explore the combined HMI and TSI for ablation treatment monitoring and the evaluation of bio-effects involved in novel ultrasound modalities such as ultrasound neuromodulation.

IV. Conclusion

This study describes an interleaving pulse sequence tested in a tissue-mimicking phantom that alternates amplitude-modulated FUS and plane-wave imaging pulses and enables the simultaneous evaluation of tissue displacement and temperature rise during sonication. A TSI processing evaluated the phantom temperature, and an HMI displacement processing evaluated the phantom tissue motion. The results indicate that FUS pulses with acoustic intensities above diagnostic ranges can operate at safe temperatures below 1°C. For temperatures below 1.8°C, the steady-state oscillation in the phantom throughout the pulse sequence indicates that the temperature does not affect the displacement estimation. Conversely, the TSI estimations were similar to simulated temperatures as opposed to thermocouple measurements that presented higher variability due to the viscous heating artifacts. The interleaved sequence indicates that the interference effects between the two techniques could be minimized, allowing the estimation of displacement and temperature simultaneously.

Acknowledgments

We thank Pablo Abreu, MS, for the administrative assistance in the project.

References

[1] W. L. Nyborg, "Acoustic Streaming near a Boundary," *J. Acoust. Soc. Am.*, vol. 30, no. 4, pp. 329–339, Apr. 1958.

[2] W. L. Nyborg, "Solutions of the bio-heat transfer equation," *Phys. Med. Biol.*, vol. 33, no. 7, pp. 785–792, Jul. 1988.

[3] M. L. Palmeri, A. C. Sharma, R. R. Bouchard, R. W. Nightingale, and K. R. Nightingale, "A finite-element method model of soft tissue response to impulsive acoustic radiation force," *IEEE Trans. Ultrason. Ferroelectr. Freq. Control*, vol. 52, no. 10, pp. 1699–1712, 2005.

[4] C. H. Seo, Y. Shi, S.-W. Huang, K. Kim, and M. O'Donnell, "Thermal strain imaging: a review," *Interface Focus*, vol. 1, no. 4, pp. 649–664, Aug. 2011.

[5] W. D. O'Brien, "Ultrasound—biophysics mechanisms," *Prog. Biophys. Mol. Biol.*, vol. 93, pp. 212–255, 2007.

[6] M. A. Abbass, J. K. Killin, N. Mahalingam, F. M. Hooi, P. G. Barthe, and T. D. Mast, "Real-Time Spatiotemporal Control of High-Intensity Focused Ultrasound Thermal Ablation Using Echo Decorrelation Imaging in ex Vivo Bovine Liver," *Ultrasound Med. Biol.*, vol. 44, no. 1, pp. 199–213, Jan. 2018.

[7] A. L. Baggio, H. A. S. Kamimura, J. Henrique Lopes, A. A. O. Carneiro, and G. T. Silva, "Parametric array signal in confocal vibro-acoustography," *Appl. Acoust.*, vol. 126, pp. 143–148, Nov. 2017.

[8] V. Barrere, D. Melodelima, S. Catheline, and B. Giammarinaro, "Imaging of Thermal Effects during High-Intensity Ultrasound Treatment in Liver by Passive Elastography: A Preliminary Feasibility in Vitro Study," *Ultrasound Med. Biol.*, vol. 46, no. 8, pp. 1968–1977, Aug. 2020.

[9] R. Bouchard, J. Dahl, S. Hsu, M. Palmeri, and G. Trahey, "Image quality, tissue heating, and frame rate trade-offs in acoustic radiation force impulse imaging," *IEEE Trans. Ultrason. Ferroelectr. Freq. Control*, vol. 56, no. 1, pp. 63–76, Jan. 2009.

[10] M. Fatemi and J. F. Greenleaf, "Vibro-acoustography: An imaging modality based on ultrasound-stimulated acoustic emission," *Proc. Natl. Acad. Sci.*, vol. 96, no. 12, pp. 6603–6608, Jun. 1999.

[11] H. Kamimura, L. Wang, A. Carneiro, R. Kinnick, K. An, and M. Fatemi, "Vibroacoustography for the assessment of total hip arthroplasty," *Clinics*, vol. 68, no. 4, pp. 463–468, Apr. 2013.

[12] Y. Hadadian, J. H. Uliana, A. A. O. Carneiro, and T. Z. Pavan, "A Novel Theranostic Platform: Integration of Magnetomotive and Thermal Ultrasound Imaging With Magnetic Hyperthermia," *IEEE Trans. Biomed. Eng.*, vol. 68, no. 1, pp. 68–77, Jan. 2021.

[13] H. A. S. Kamimura, A. Conti, N. Toschi, and E. E. Konofagou, "Ultrasound Neuromodulation: Mechanisms and the Potential of Multimodal Stimulation for Neuronal Function Assessment," *Front. Phys.*, vol. 8, p. 150, May 2020.

[14] N. McDannold and S. E. Maier, "Magnetic resonance acoustic radiation force imaging," *Med. Phys.*, vol. 35, no. 8, pp. 3748–3758, Jul. 2008.

[15] B. Larrat *et al.*, "MR-guided transcranial brain HIFU in small animal models," *Phys. Med. Biol.*, vol. 55, no. 2, pp. 365–388, Jan. 2010.

[16] M. A. Phipps *et al.*, "Considerations for ultrasound exposure during transcranial MR acoustic radiation force imaging," *Sci. Rep.*, vol. 9, no. 1, p. 16235, Dec. 2019.

[17] J. De Poorter, "Noninvasive MRI thermometry with the proton resonance frequency method: Study of susceptibility effects," *Magn. Reson. Med.*, vol. 34, no. 3, pp. 359–367, Sep. 1995.

[18] N. McDannold, N. Vykhodtseva, F. A. Jolesz, and K. Hynynen, "MRI Investigation of the Threshold for Thermally Induced Blood-Brain Barrier Disruption and Brain Tissue Damage in the Rabbit Brain," *Magn. Reson. Med.*, vol. 51, no. 5, pp. 913–923, 2004.

[19] M. O. Köhler *et al.*, "Volumetric HIFU ablation under 3D guidance of rapid MRI thermometry," *Med. Phys.*, vol. 36, no. 8, pp. 3521–3535, Aug. 2009.

[20] C. D. Arvanitis and N. McDannold, "Integrated ultrasound and magnetic resonance imaging for simultaneous temperature and cavitation monitoring during focused ultrasound therapies.," *Med. Phys.*, vol. 40, no. 11, p. 112901, 2013.

[21] J. T. de Bever, H. Odéen, L. W. Hofstetter, and D. L. Parker, "Simultaneous MR thermometry and acoustic radiation force imaging using interleaved acquisition," *Magn. Reson. Med.*, vol. 79, no. 3, pp. 1515–1524, Mar. 2018.

[22] J. D. Achenbach, "Elastodynamic theory," in *Wave Propagation in Elastic Solids*, 1973rd ed., H. A. Lauwerier and W. T. Koiter, Eds. Amsterdam: Elsevier Science Publishers B.V., 1973, pp. 79–121.

[23] E. Konofagou, J. Thierman, and K. Hynynen, "A focused ultrasound method for simultaneous diagnostic and therapeutic applications—a simulation study," *Phys. Med. Biol.*, vol. 46, no. 11, pp. 2967–2984, Nov. 2001.

[24] C. Maleke, M. Pernot, and E. E. Konofagou, "Single-element focused ultrasound transducer method for harmonic motion imaging," *Ultrason. Imaging*, vol. 28, pp. 144–158, 2006.

[25] C. Maleke and E. E. Konofagou, "In Vivo Feasibility of Real-Time Monitoring of Focused Ultrasound Surgery (FUS) Using Harmonic Motion Imaging (HMI)," *IEEE Trans. Biomed. Eng.*, vol. 57, no. 1, pp. 7–11, Jan. 2010.

[26] G. Y. Hou, F. Marquet, S. Wang, and E. E. Konofagou, "Multi-parametric monitoring and assessment of high-intensity focused ultrasound (HIFU) boiling by harmonic motion imaging for focused ultrasound (HMIFU): an *ex vivo* feasibility study," *Phys. Med. Biol.*, vol. 59, no. 5, pp. 1121–1145, Mar. 2014.

[27] J. Vappou, C. Maleke, and E. E. Konofagou, "Quantitative viscoelastic parameters measured by harmonic motion imaging," *Phys. Med. Biol.*, vol. 54, no. 11, pp. 3579–3594, Jun. 2009.

[28] N. Saharkhiz *et al.*, "Harmonic motion imaging of human breast masses: an in vivo clinical feasibility," *Sci. Rep.*, vol. 10, no. 1, p. 15254, Dec. 2020.

[29] A. Nabavizadeh *et al.*, "Noninvasive Young's modulus visualization of fibrosis progression and delineation of pancreatic ductal adenocarcinoma (PDAC) tumors using Harmonic Motion Elastography (HME) in vivo," *Theranostics*, vol. 10, no. 10, pp. 4614–4626, 2020.

[30] T. Payen *et al.*, "Harmonic Motion Imaging of Pancreatic Tumor Stiffness Indicates Disease State and Treatment Response," *Clin. Cancer Res.*, vol. 26, no. 6, pp. 1297–1308, Mar. 2020.

[31] Y. Han, S. Wang, H. Hibshoosh, B. Taback, and E. Konofagou, "Tumor characterization and treatment monitoring of postsurgical human breast specimens using harmonic motion imaging (HMI)," *Breast Cancer Res.*, vol. 18, no. 1, p. 46, Dec. 2016.

[32] J.-L. Dillenseger and S. Esneault, "Fast FFT-based bioheat transfer equation computation," *Comput. Biol. Med.*, vol. 40, no. 2, pp. 119–123, 2010.

[33] H. H. Pennes, "Analysis of Tissue and Arterial Blood Temperatures in the Resting Human Forearm," *J. Appl. Physiol.*, vol. 1, no. 2, pp. 93–122, Aug. 1948.

[34] W. L. Nyborg *et al.*, "Exposure criteria for medical diagnostic

ultrasound : I, Criteria based on thermal mechanisms : recommendations of the National Council on Radiation Protection and Measurements," The Council, Bethesda, MD, 1992.

[35] V. Suomi, Y. Han, E. Konofagou, and R. O. Cleveland, "The effect of temperature dependent tissue parameters on acoustic radiation force induced displacements," *Phys. Med. Biol.*, vol. 61, no. 20, pp. 7427–7447, Oct. 2016.

[36] A. Anand, D. Savery, and C. Hall, "Three-dimensional spatial and temporal temperature imaging in gel phantoms using backscattered ultrasound," *IEEE Trans. Ultrason. Ferroelectr. Freq. Control*, vol. 54, no. 1, pp. 23–31, Jan. 2007.

[37] M. J. Daniels, T. Varghese, E. L. Madsen, and J. A. Zagzebski, "Non-invasive ultrasound-based temperature imaging for monitoring radiofrequency heating—phantom results," *Phys. Med. Biol.*, vol. 52, no. 16, pp. 4827–4843, Aug. 2007.

[38] R. Maass-Moreno, C. A. Damianou, and N. T. Sanghvi, "Noninvasive temperature estimation in tissue via ultrasound echo-shifts. Part I. Analytical model," *J. Acoust. Soc. Am.*, vol. 100, no. 4, pp. 2514–2521, Oct. 1996.

[39] R. Maass-Moreno, C. A. Damianou, and N. T. Sanghvi, "Noninvasive temperature estimation in tissue via ultrasound echo-shifts. Part II. In vitro study," *J. Acoust. Soc. Am.*, vol. 100, no. 4, pp. 2522–2530, Oct. 1996.

[40] E. S. Ebbini, C. Simon, and D. Liu, "Real-Time Ultrasound Thermography and Thermometry [Life Sciences]," *IEEE Signal Process. Mag.*, vol. 35, no. 2, pp. 166–174, Mar. 2018.

[41] S. A. Lee, H. A. S. Kamimura, and E. E. Konofagou, "Displacement imaging during focused ultrasound median nerve modulation: A preliminary study in human pain sensation mitigation," *IEEE Trans. Ultrason. Ferroelectr. Freq. Control*, pp. 1–1, 2020.

[42] S. A. Lee, H. A. S. Kamimura, M. T. Burgess, and E. E. Konofagou, "Displacement Imaging for Focused Ultrasound Peripheral Nerve Neuromodulation," *IEEE Trans. Med. Imaging*, vol. 39, no. 11, 2020.

[43] H. A. S. Kamimura, C. Aurup, E. V Bendau, N. Saharkhiz, M. G. Kim, and E. E. Konofagou, "Iterative Curve Fitting of the Bioheat Transfer Equation for Thermocouple-Based Temperature Estimation In Vitro and In Vivo," *IEEE Trans. Ultrason. Ferroelectr. Freq. Control*, vol. 67, no. 1, pp. 70–80, Jan. 2020.

[44] A. M. Pouch, T. W. Cary, S. M. Schultz, and C. M. Sehgal, "In Vivo Noninvasive Temperature Measurement by B-Mode Ultrasound Imaging," *J. Ultrasound Med.*, vol. 29, no. 11, pp. 1595–1606, Nov. 2010.

[45] T. A. Fuhrmann, O. Georg, J. Haller, K.-V. Jenderka, and V. Wilkens, "Uncertainty estimation for temperature measurement with diagnostic ultrasound," *J. Ther. Ultrasound*, vol. 4, no. 1, p. 28, Dec. 2016.

[46] B. E. Treeby and B. T. Cox, "k-Wave: MATLAB toolbox for the simulation and reconstruction of photoacoustic wave fields," *J. Biomed. Opt.*, vol. 15, no. 2, p. 021314, 2010.

[47] B. Gao, S. Langer, and P. M. Corry, "Application of the time-dependent Green's function and Fourier transforms to the solution of the bioheat equation," *Int. J. Hyperth.*, vol. 11, no. 2, pp. 267–285, Jan. 1995.

[48] A. Dabbagh, B. J. J. Abdullah, C. Ramasindarum, and N. H. Abu Kasim, "Tissue-Mimicking Gel Phantoms for Thermal Therapy Studies," *Ultrason. Imaging*, vol. 36, no. 4, pp. 291–316, Oct. 2014.

[49] J. Foiret and K. W. Ferrara, "Spatial and Temporal Control of Hyperthermia Using Real Time Ultrasonic Thermal Strain Imaging with Motion Compensation, Phantom Study," *PLoS One*, vol. 10, no. 8, p. e0134938, Aug. 2015.

[50] W. J. Fry and R. B. Fry, "Determination of Absolute Sound Levels and Acoustic Absorption Coefficients by Thermocouple Probes—Experiment," *J. Acoust. Soc. Am.*, vol. 26, no. 3, pp. 311–317, May 1954.

[51] W. J. Fry and R. B. Fry, "Determination of Absolute Sound Levels and Acoustic Absorption Coefficients by Thermocouple Probes—theory," *J. Acoust. Soc. Am.*, vol. 26, no. 3, pp. 311–317, May 1954.

[52] E. Martin and B. Treeby, "Investigation of the repeatability and reproducibility of hydrophone measurements of medical ultrasound fields," *J. Acoust. Soc. Am.*, vol. 145, no. 3, pp. 1270–1282, Mar. 2019.

[53] J. Chen, G. Y. Hou, F. Marquet, Y. Han, F. Camarena, and E. Konofagou, "Radiation-force-based estimation of acoustic attenuation using harmonic motion imaging (HMI) in phantoms and in vitro livers before and after HIFU ablation," *Phys. Med. Biol.*, vol. 60, no. 19, pp. 7499–7512, Oct. 2015.

[54] K. Nightingale, "Acoustic Radiation Force Impulse (ARFI) Imaging: A Review," *Curr. Med. Imaging Rev.*, vol. 7, no. 4, pp. 328–339, Nov. 2011.

[55] T. Tiennot, H. A. S. Kamimura, S. A. Lee, C. Aurup, and E. E. Konofagou, "Numerical modeling of ultrasound heating for the correction of viscous heating artifacts in soft tissue temperature measurements," *Appl. Phys. Lett.*, vol. 114, no. 20, 2019.

[56] J. Grondin, T. Payen, S. Wang, and E. E. Konofagou, "Real-time Monitoring of High Intensity Focused Ultrasound (HIFU) Ablation of In Vitro Canine Livers Using Harmonic Motion Imaging for Focused Ultrasound (HMIFU)," *J. Vis. Exp.*, 2015.

[57] H. Chen *et al.*, "Harmonic motion imaging for abdominal tumor detection and high-intensity focused ultrasound ablation monitoring: an in vivo feasibility study in a transgenic mouse model of pancreatic cancer," *IEEE Trans. Ultrason. Ferroelectr. Freq. Control*, vol. 62, no. 9, pp. 1662–1673, Sep. 2015.

[58] G. Y. Hou, F. Marquet, S. Wang, I.-Z. Apostolakis, and E. E. Konofagou, "High-intensity focused ultrasound monitoring using harmonic motion imaging for focused ultrasound (HMIFU) under boiling or slow denaturation conditions," *IEEE Trans. Ultrason. Ferroelectr. Freq. Control*, vol. 62, no. 7, pp. 1308–1319, Jul. 2015.

[59] C. Maleke and E. E. Konofagou, "Harmonic motion imaging for focused ultrasound (HMIFU): a fully integrated technique for sonication and monitoring of thermal ablation in tissues," *Phys. Med. Biol.*, vol. 53, no. 6, pp. 1773–1793, Mar. 2008.

[60] C. A. Damianou, N. T. Sanghvi, F. J. Fry, and R. Maass-Moreno, "Dependence of ultrasonic attenuation and absorption in dog soft tissues on temperature and thermal dose," *J. Acoust. Soc. Am.*, vol. 102, no. 1, pp. 628–634, Jul. 1997.

[61] C. W. Connor and K. Hynynen, "Bio-acoustic thermal lensing and nonlinear propagation in focused ultrasound surgery using large focal spots: a parametric study," *Phys. Med. Biol.*, vol. 47, no. 11, p. 306, Jun. 2002.

[62] M. G. Shapiro, K. Homma, S. Villarreal, C.-P. Richter, and F. Bezanilla, "Infrared light excites cells by changing their electrical capacitance," *Nat. Commun.*, vol. 3, p. 736, 2012.

[63] M. M. Elwassif, Q. Kong, M. Vazquez, and M. Bikson, "Bio-Heat Transfer Model of Deep Brain Stimulation Induced Temperature changes," in *2006 International Conference of the IEEE Engineering in Medicine and Biology Society*, 2006, pp. 3580–3583.

[64] R. Janca *et al.*, "Intraoperative Thermography of the Electrical Stimulation Mapping: A Safety Control Study," *IEEE Trans. Neural Syst. Rehabil. Eng.*, vol. 26, no. 11, pp. 2126–2133, Nov. 2018.

[65] M. G. Kim, H. A. S. Kamimura, S. A. Lee, C. Aurup, N. Kwon, and E. E. Konofagou, "Image-guided focused ultrasound modulates electrically evoked motor neuronal activity in the mouse peripheral nervous system in vivo," *J. Neural Eng.*, Jan. 2020.

[66] T. Heimburg and A. D. Jackson, "On soliton propagation in biomembranes and nerves," *Proc. Natl. Acad. Sci.*, vol. 102, no. 28, pp. 9790–9795, Jul. 2005.

[67] H. A. S. Kamimura *et al.*, "Focused ultrasound neuromodulation of cortical and subcortical brain structures using 1.9 MHz," *Med. Phys.*, vol. 43, no. 10, pp. 5730–5735, Sep. 2016.

[68] C. Aurup, H. A. S. Kamimura, and E. E. Konofagou, "High-Resolution, Focused Ultrasound-Mediated Neuromodulation and Detailed Analysis of Electromyography Characteristics Reveals a High Degree of Spatial Specificity in Elicited Responses in Mice in Vivo," in *IEEE International Ultrasonics Symposium, IUS*, 2018, vol. 2018-Octob.

[69] M. E. Downs, S. A. Lee, G. Yang, S. Kim, Q. Wang, and E. E. Konofagou, "Non-invasive peripheral nerve stimulation via focused ultrasound in vivo," *Phys. Med. Biol.*, vol. 63, no. 3, p. 035011, Jan. 2018.

[70] T. A. Fuhrmann, O. Georg, J. Haller, K.-V. Jenderka, and V. Wilkens, "Uncertainty estimation for temperature measurement with diagnostic ultrasound," *J. Ther. Ultrasound*, vol. 4, no. 1, p. 28, Dec. 2016.

Hermes A. S. Kamimura (M'16) received the B.S. degree in medical physics and the M.S. and Ph.D. degrees in physics applied to medicine and biology from the University of São Paulo, Ribeirão Preto, Brazil, in 2008, 2011, and 2016, respectively. He conducted research projects in therapeutic and ultrasound imaging at Mayo Clinic, Rochester, MN, USA, in 2010, and Columbia University, New York, NY, USA, in 2014, in student exchange programs. He was a Postdoctoral Research Scientist with the French Alternative Energies and Atomic Energy Commission (CEA), Gif-sur-Yvette, France, and Columbia University, where he is currently an Associate Research Scientist. His research interests include harmonic motion imaging and therapeutic ultrasound spanning both ultrasound neuromodulation and ultrasound-mediated blood-brain barrier disruption for targeted drug delivery in the central nervous system. Dr. Kamimura is a member of the Acoustical Society of America, the Brazilian Physical Society, and the Brazilian Society of Biomedical Engineering. He was a recipient of the Outstanding Reviewer Award for Physics in Medicine and Biology, IOP Publishing in 2018, and the Best Ph.D. Dissertation Award in the field of medical physics in 2016 by the Brazilian Physical Society. He served as a Topic Editor for Frontiers in Physics and Frontiers in Physiology (2019-2021).

Niloufar Saharkhiz was born in Tehran, Iran, in 1991. She received the B.S. degree in electrical engineering with a major in electronics from Iran University of Science and Technology (IUST), Tehran, Iran, in 2014, and the M.Sc. degree in biomedical engineering with a major in medical physics from Imperial College London, London, U.K., in 2015. She is currently pursuing a Ph.D. degree in biomedical engineering with Columbia University, New York City, NY, USA. She is with the Elasticity Imaging and Ultrasound Laboratory (UEIL), and her current research interests include diagnosis and treatment monitoring of breast cancer using Harmonic Motion Imaging.

Stephen A. Lee received the bachelor's degree from the University of North Carolina at Chapel Hill, Chapel Hill, NC, USA in 2015, and the Master's of Science and Master's of philosophy degree from Columbia University, New York, NY, USA, in 2018 and 2019. He is currently enrolled in the doctoral program with the Department of Biomedical Engineering, Columbia University, New York, NY, USA, where he is currently working towards his Ph.D. His current research interests include studying the mechanism of ultrasound neuromodulation and how ultrasound imaging techniques, such as functional ultrasound, can be used to understand this phenomenon.

Elisa E. Konofagou (S'98–A'99–M'03) is currently the Robert and Margaret Hariri Professor of biomedical engineering and a Professor of radiology as well as the Director of the Ultrasound and Elasticity Imaging Laboratory with the Biomedical Engineering Department, Columbia University, New York, NY, USA. She has co-authored over 220 peer-reviewed journal articles. Her current research interests include the development of novel elasticity imaging techniques and therapeutic ultrasound methods and, more notably, myocardial elastography, electromechanical and pulse wave imaging, harmonic motion imaging, focused ultrasound therapy, and drug delivery in the brain, with several clinical collaborations in the Columbia Presbyterian Medical Center, New York, NY, USA, and elsewhere.

Prof. Konofagou was a recipient of awards, such as the CAREER Award from the National Science Foundation and the Nagy Award from the National Institutes of Health as well as others from the American Heart Association, the Acoustical Society of America, the American Institute of Ultrasound in Medicine, the Wallace H. Coulter Foundation, the Bodossaki Foundation, the Society of Photo-Optical Instrumentation Engineers, and the Radiological Society of North America. She is a Technical Committee Member of the Acoustical Society of America, the International Society of Therapeutic Ultrasound, the IEEE Engineering in Medicine and Biology Conference, the IEEE International Ultrasonics Symposium, and the American Association of Physicists in Medicine. She serves as an Associate Editor for the IEEE Transactions On Ultrasonics, Ferroelectrics, And Frequency Control, Ultrasonic Imaging, and Medical Physics.